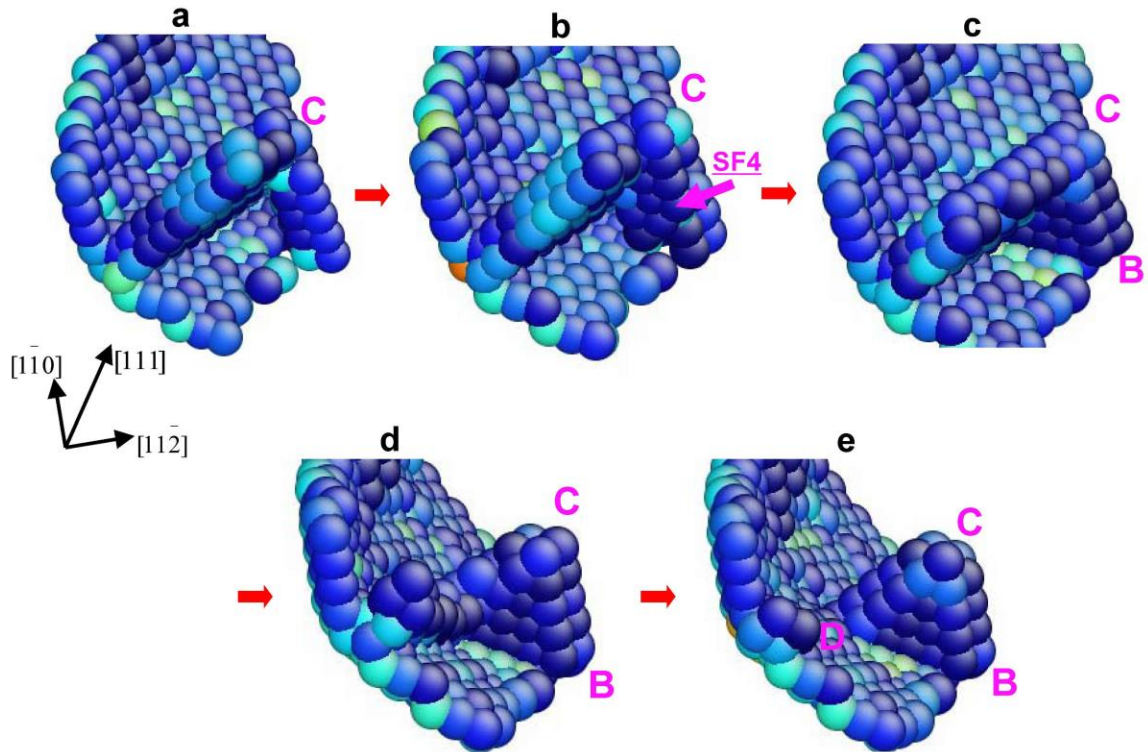
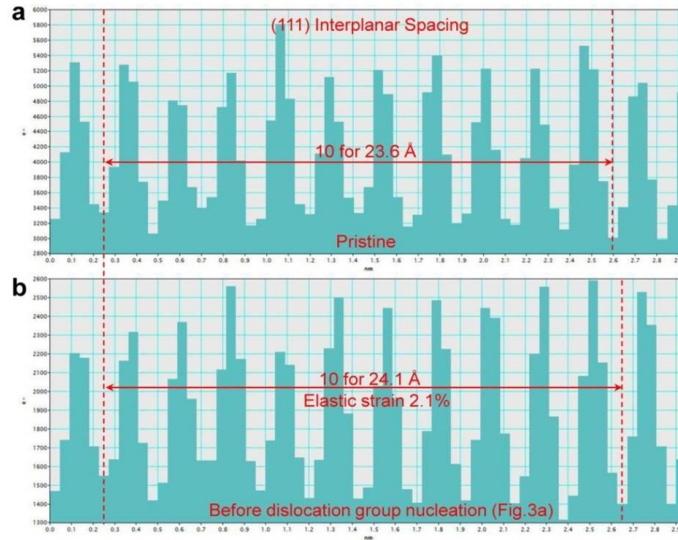


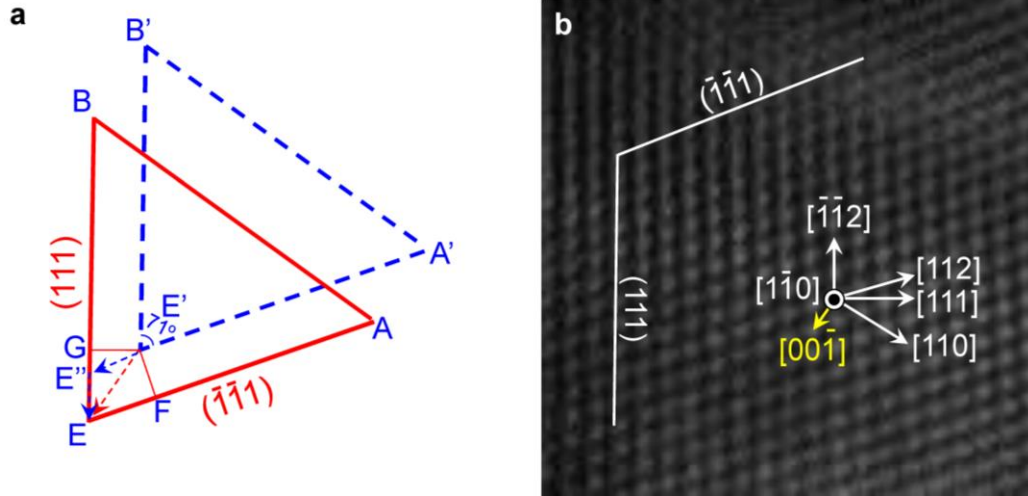
**Supplementary Figure S1. Morphology and structure of stacking fault tetrahedra (SFT).** (a) The morphology of SFT in 3D space, which is composed of stacking faults (SFs) and stair-rod dislocations on four inclined  $\{111\}$  planes. (b) The projection view ( $\triangle ABE$ ) of SFT along the  $[\bar{1}\bar{1}0]$  direction, which is an isosceles triangle with a  $71^\circ$  apex angle. The blue triangle is the shape of the triangular defect observed in Fig. 1f after rotation by  $90^\circ$ . Careful comparisons indicate that the triangular defect observed in Fig. 1f is the same as the projection view of SFT along the  $[\bar{1}\bar{1}0]$  direction, in both shape and angles. (c-d) Comparison of SFT between experiment and molecular dynamics (MD) simulation. (c) Reproduced image of Fig. 1f after rotation by  $90^\circ$ . Scale bar, 5 nm. (d) MD snapshot of Fig. 2e. In (c-d), the  $\{111\}$  faces of the SFT are indicated by dashed lines. (e) The SFs in a dislocation-origined SFT are labelled out along  $\langle 112 \rangle$  direction on two  $\{111\}$  planes, which is consistent with the one shown in Fig. 1f. Moreover, it should be noted that the SFT is the reaction product of four closely-spaced dislocations and part of the SFs have been removed by trailing partials during the SFT formation process (Fig. 2c,g). As a result, the width of SFs on the SFT should conceivably differ from the spacing between the leading and trailing partials of a stand-alone dislocation.



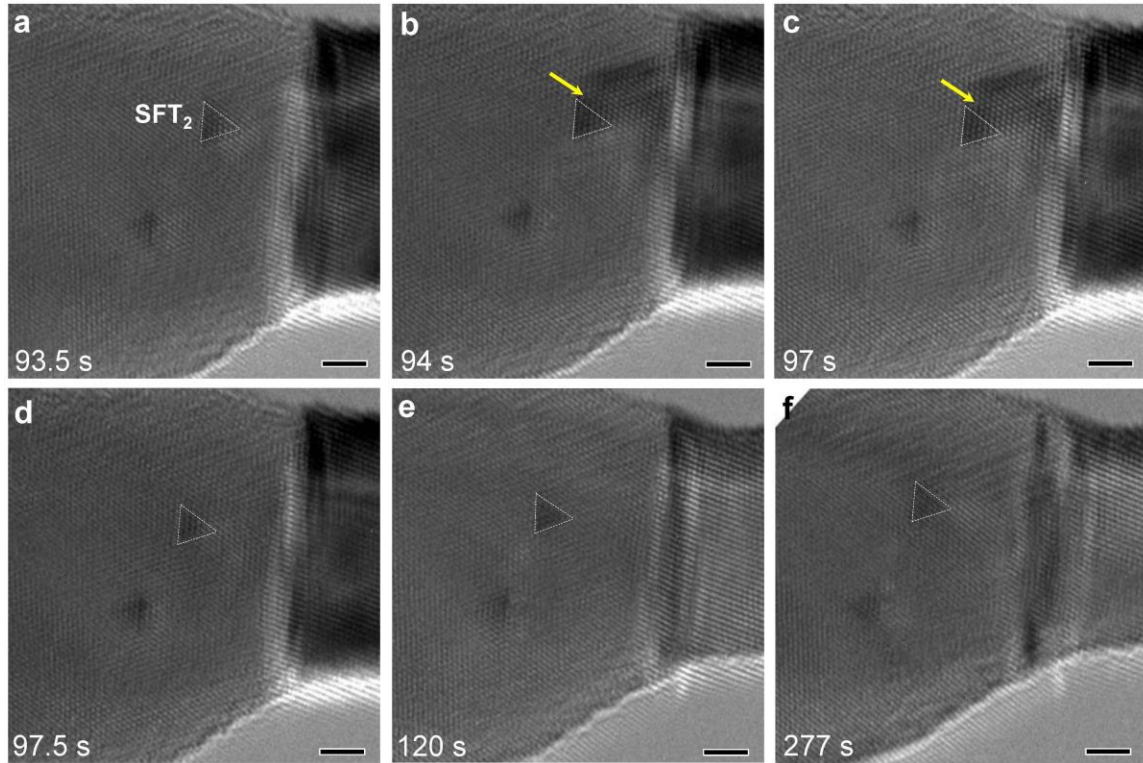
**Supplementary Figure S2. Formation of a closed-SFT through the cross-slip of a trailing partial.** (a) The initial open-SFT formed by the interactions of partial dislocations, as in Fig. 2c in the main text. (b)  $SF_4$  propagates into the open  $(111)$  plane through the cross-slip of a trailing partial in Fig. 2g in the main text. (c-d) The propagation of  $SF_4$  removes the trails of the initial open-SFT and produces the fourth face of the SFT. (e) The base BCD of the SFT in Fig. 2d, is fully formed making it a closed-SFT.



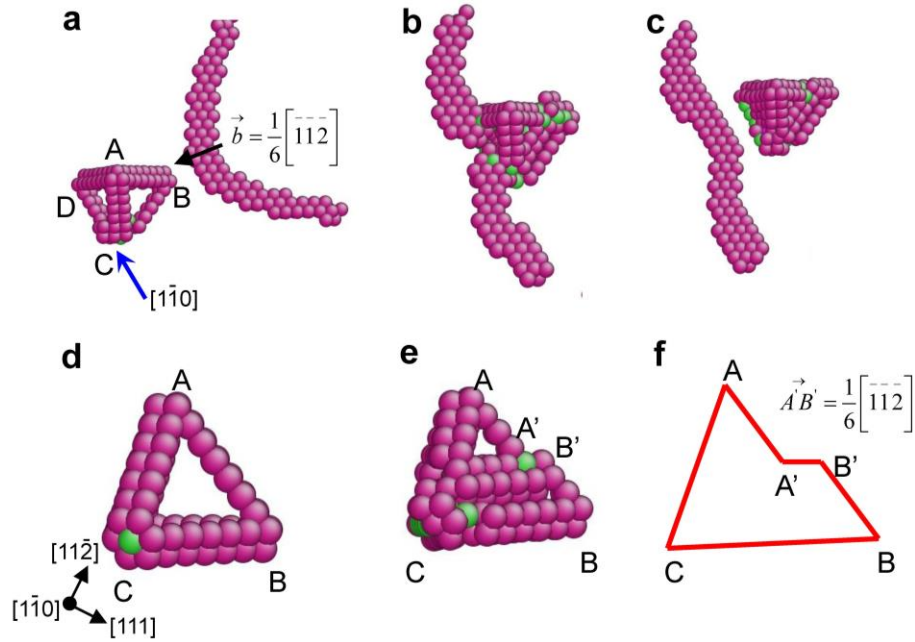
**Supplementary Figure S3. Estimation of the nucleation stress of the partial dislocation group.** The stress in Au nanowires can be estimated by measuring the change of interplanar spacing of the (111) plane (perpendicular to the loading direction) during tensile deformation. **(a)** In the pristine Au nanowire, the interplanar spacing is 2.36 Å. Under mechanical loading, the elastic strain causes an increase of interplanar spacing. **(b)** Before the nucleation of dislocations, the (111) interplanar spacing is increased to ~ 2.41 Å, corresponding to an elastic strain of 2.1%. A previous study shows that Young's modulus along the [111] direction of Au single crystal is about ~110 GPa (Ref. 41). Thus the nucleation stress of the dislocation is estimated as ~2.3 GPa.



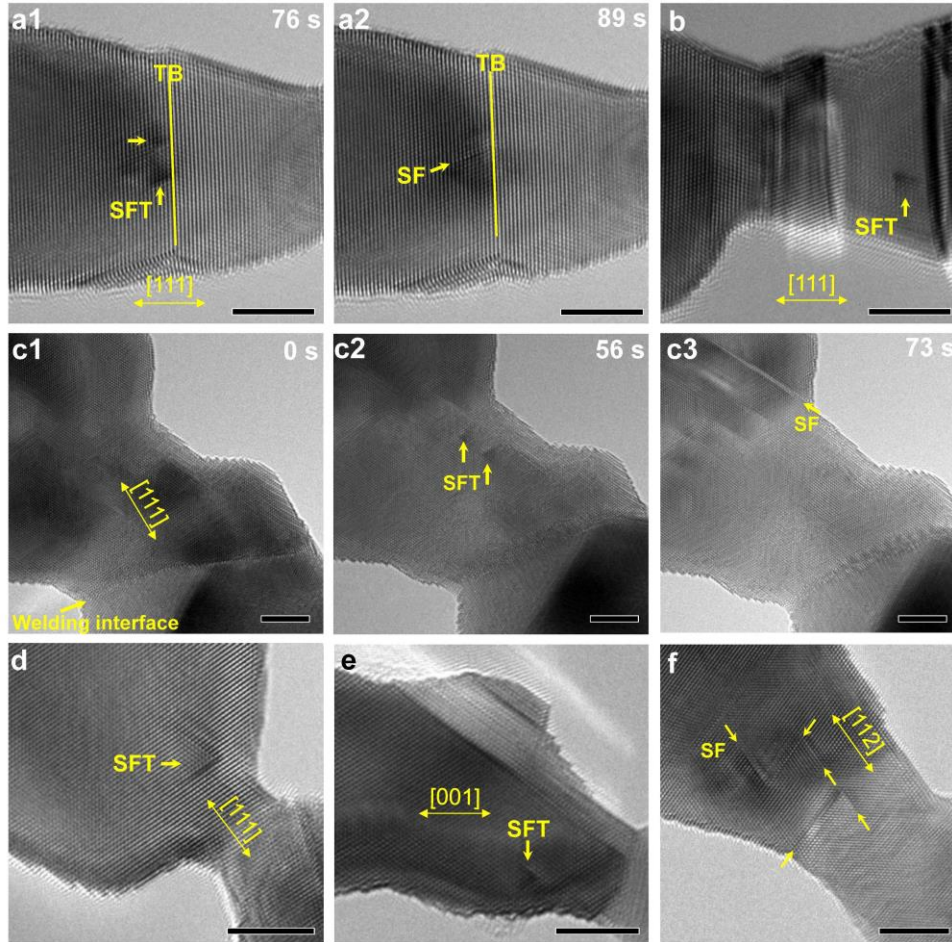
**Supplementary Figure S4. Migration direction of SFT<sub>2</sub> under the tensile loading.** (a) Schematic illustration of the migration direction of SFT<sub>2</sub>.  $\Delta A'B'E'$  with a  $71^\circ$  apex angle is the projection view of SFT<sub>2</sub> along the  $[\bar{1}\bar{1}0]$  direction.  $A'E'$  and  $B'E'$  is the projection view of two sets of  $\{111\}$  planes, respectively. (b) The crystal orientation of an Au nanocrystal, which has the same orientation as the one in Fig. 4 of the main text. According to the experimental measurement (Fig. 4), the SFT<sub>2</sub> can migrate on both  $(111)$  and  $(\bar{1}\bar{1}\bar{1})$  planes simultaneously with the same displacements. Thus, the migration process can be decomposed into two steps: firstly, the SFT<sub>2</sub> migrates on  $(\bar{1}\bar{1}\bar{1})$  plane along the  $[\bar{1}\bar{1}\bar{2}]$  direction for one atomic layer, *i.e.* from  $E'$  to  $E''$ ; finally, the SFT<sub>2</sub> migrates on  $(111)$  plane along the  $[11\bar{2}]$  direction for one atomic layer, *i.e.* from  $E''$  to  $E$ . After these two steps,  $E'$  will move to  $E$  with the same displacements on both  $(111)$  and  $(\bar{1}\bar{1}\bar{1})$  planes. Therefore, the migration direction is  $E'E$ , which is  $[\bar{1}\bar{1}\bar{2}] + [11\bar{2}] \rightarrow [00\bar{1}]$ . The migration direction of SFT<sub>2</sub> is marked out in the real crystal by a yellow arrow in (b).



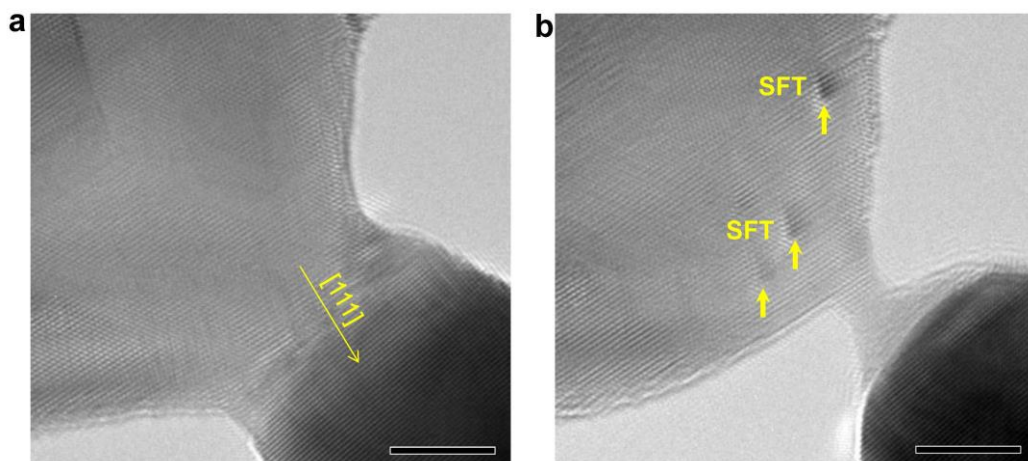
**Supplementary Figure S5. Comparison of the size of SFT<sub>2</sub> before and after migration.** (a) TEM image of Fig. 4a, (b) image of Fig. 4b, (c) image of Fig. 4d, (d) image of Fig. 4e, (e) an additional image showing the SFT size at 120 s, and (f) image of Fig. 4f. Scale bar in (a-f), 2 nm. The yellow arrows in (b-c) indicate the strain contrast induced by dislocation-SFT<sub>2</sub> interaction. It can be seen that the size of this moving SFT (marked as SFT<sub>2</sub>) does not change before and after migration (a and d-f). When watching Supplementary Movie 2, to some extent, it shows a visual trick of change of the size of SFT<sub>2</sub>, due to the strain contrast induced by dislocation-SFT<sub>2</sub> interaction as pointed out by the yellow arrows in (b-c). After the dislocation group nucleates and interacts with SFT<sub>2</sub>, the strain-induced contrast accumulates at the edge of SFT<sub>2</sub>, which makes the size of SFT<sub>2</sub> look slightly larger than the pristine one. This strain contrast disappears as the group of dislocations glides away, causing a visual trick of change of the size of SFT<sub>2</sub>, which actually not. Moreover, the change in the number of atomic layers between the two SFT in Fig. 4 indicates that the SFT<sub>2</sub> is migrating during the SFT-dislocation interaction; it is the same SFT but not a newly generated one. However, due to the relatively low resolution of Supplementary Movie 2 and small displacement of SFT<sub>2</sub>, the migration of SFT<sub>2</sub> is not so significant in the movie as that shown in the zoomed-in images of Fig. 4.



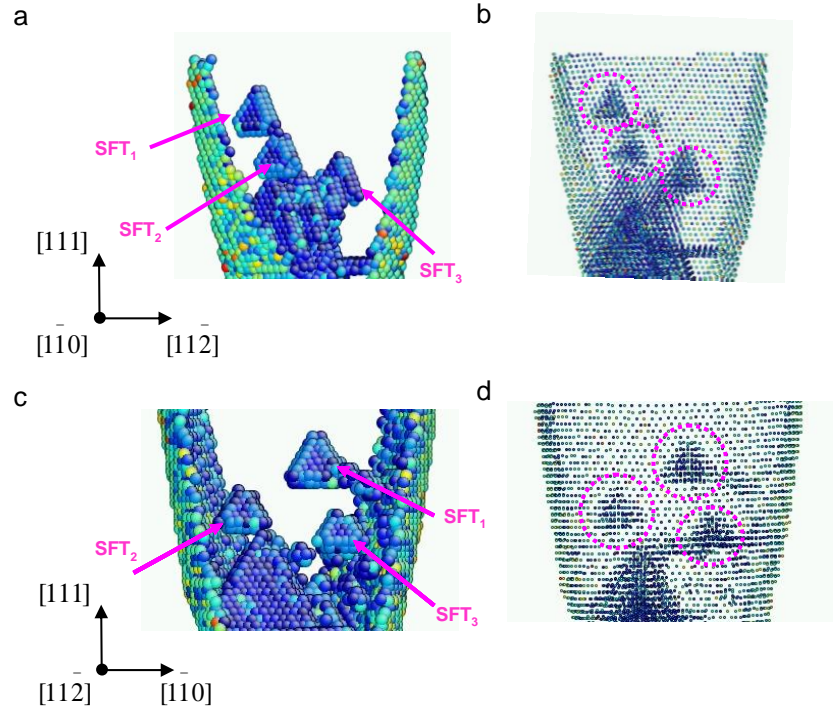
**Supplementary Figure S6. Interaction of a partial dislocation with SFT and the surface step on SFT created by the interaction. (a-c)** The dislocation-SFT interaction process. The dislocation is a partial dislocation with burgers vector of  $\frac{1}{6}[\bar{1}\bar{1}\bar{2}]$ . **(d-e)** The ABC face of the SFT, before and after the dislocation-SFT interaction, clearly depicting the surface step in the direction of its burgers vector. **(f)** Schematic of (e).



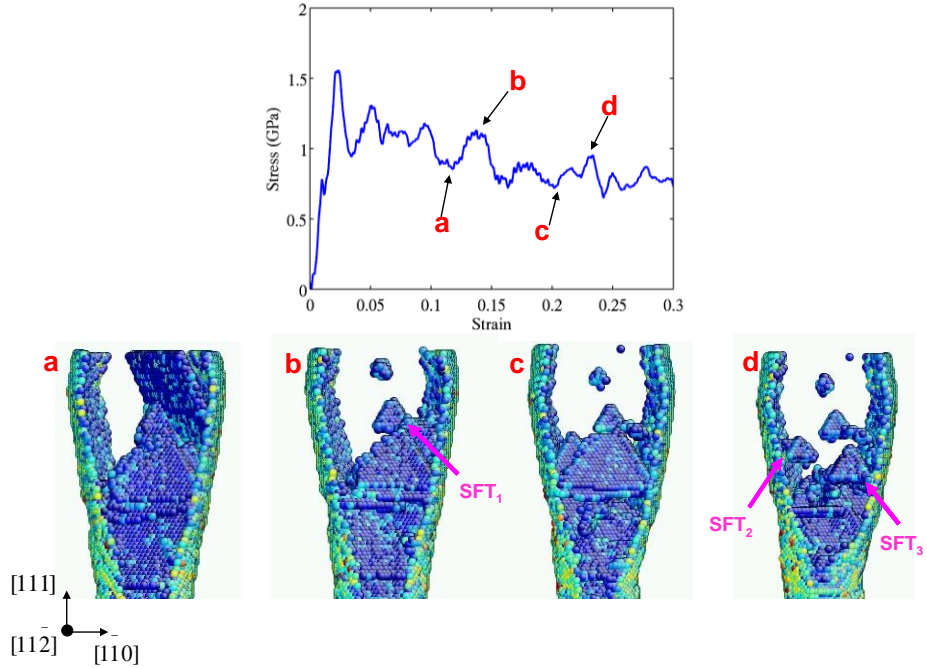
**Supplementary Figure S7. Additional examples of dislocation-origined SFT and dislocation interactions observed in different samples under tensile loading.** The sizes of samples range in between 10~30 nm and they were loaded along different directions (e.g., [111], [001], [112]). Scale bar in (a-f), 5 nm. **(a)** Annihilation of dislocation-origined SFT in Au nanowire. Under [111] tensile loading, the dislocation-origined SFT are formed near a twin boundary (TB). Further deformation induces the annihilation of SFT. The SF left in (a2) indicates that the SFT annihilation process is mediated by the dislocation-SFT interactions. **(b)** A dislocation-origined SFT formed during the necking process of a nanotwinned Au nanowire. **(c)** Generation and annihilation of dislocation-origined SFT in a sample made by cold-welding. The sample is loaded along the [111] direction. A welding interface was created in the sample due to the mismatch of geometry and orientation, as marked by the yellow arrow in (c1). **(d)** A dislocation-origined SFT formed in another [111]-loaded sample made by cold-welding. **(e)** A dislocation-origined SFT observed in a [001]-loaded sample made by cold-welding. **(f)** Dislocation interactions in an Au nanowire under the [112] loading.



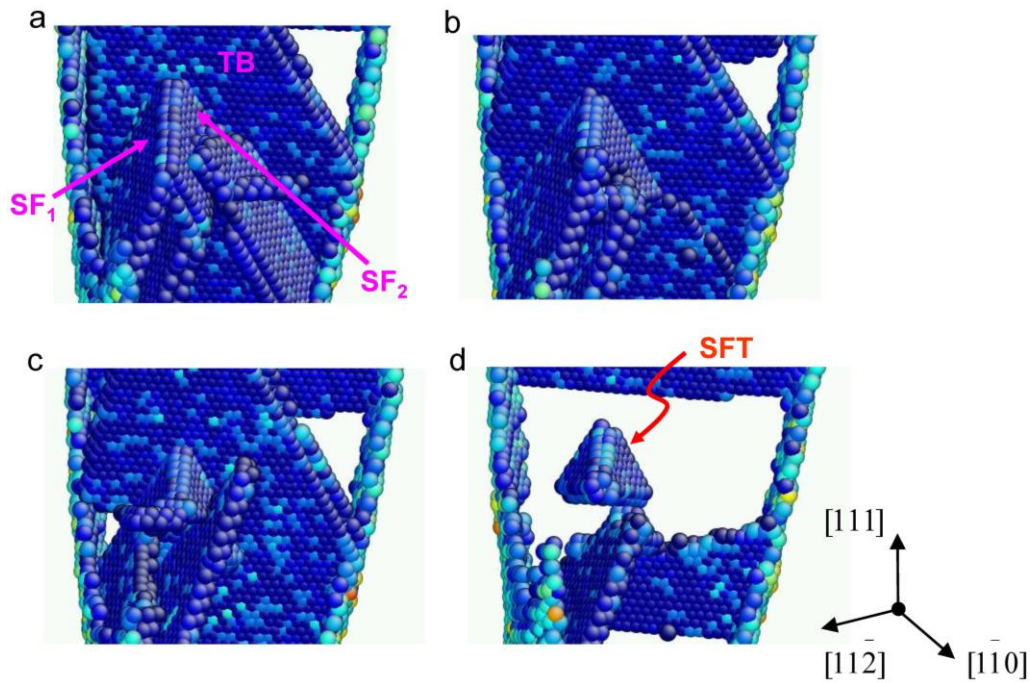
**Supplementary Figure S8. SFT observed in tensile experiment conducted under beam-blank. (a) Pristine sample. (b) Sample after beam-blank deformation.** Scale bar, 5 nm. The sample is loaded along the [111] direction. Similarly, SFT are observed to be formed during deformation without any beam irradiation and beam-induced temperature rise. Therefore, the beam-blank experiment confirms that the SFT observed during plastic deformation is indeed dislocation-originated and not vacancy-originated, and our large-scale MD simulations lend a direct support to this mechanism.



**Supplementary Figure S9. Formation of multiple SFT in a larger Au nanowire.** The Au nanowire is a double conical in shape and of 10 nm and 6 nm in diameters, respectively. In order to demonstrate that SFT are fully developed but not inter-connected, (a-b) show the atomic configurations viewed from the  $\langle 110 \rangle$  direction, and (c-d) from the  $\langle 112 \rangle$  direction.



**Supplementary Figure S10. Stress-strain curve for an Au nanowire under uniaxial tension and the MD snapshots at various strain levels.** The Au nanowire is double conical in shape, 28.26 nm long, and the diameters being 10 nm and 6 nm, respectively. Here, we note that one should ignore the first high peak, which is well-known to be caused by the high elastic stress required for nucleation of surface dislocations in a pristine nanowire. In other words, one should look into the stress-strain response beyond the first yield peak in order to understand the hardening response in MD. The several major ups and downs in the post-yield stress-strain behavior are due to hardening by dislocation interactions and SFT formation, and softening due to surface nucleation events. For example, the snapshot (a) is the beginning stage of the formation of SFT through dislocation interactions and at snapshot (b) the SFT<sub>1</sub> is fully formed. The corresponding points are marked in the stress-strain curve and it can be seen that the formation of SFT involves a rise in the stress level, indicating hardening. The same sequences of events are repeated between snapshot (c) and snapshot (d) during the formation of SFT<sub>2</sub> and SFT<sub>3</sub> (as seen in snapshot d). The resultant hardening can also be seen in the stress-strain curve.



**Supplementary Figure S11. Formation of SFT in MD simulation of a deformed Cu nanowire through the same mechanism explained in Fig. 2.** The simulation methodology and the shape and the dimensions of Cu nanowires are similar to those for Au nanowires. It is observed that SFT were formed in the Cu nanowire, following the sequence of dislocation interactions, as in Au nanowires. The initial open-SFT is formed by the locking of the partial dislocations as can be seen in (a). As in Fig. 2(b-c) only two of the three SFs constituting the open-SFT are seen in this viewing angle. Trailing partials nucleate and sweep out a part of SF<sub>1</sub> and SF<sub>2</sub> in (b) and (c), respectively. Subsequent cross-slip of the trailing partial occurs to form the fourth (basal) face and the complete SFT is formed as shown in (d).

**Supplementary Table S1. Summary of the SFT formation in 11 samples of Au nanocrystals tested in this work.**

Samples	Orientation	Samples tested	With SFT	Without SFT
Pristine nanowire	[111]	5	4	1 (dislocation interaction)
Cold-welded nanowire	[111]	4 (One beam-blank experiment)	4	0
	[001]	1	1	0
	[112]	1	0	1 (dislocation interaction)

The specific loading conditions and deformation behaviors of samples are summarized in Supplementary Table S1. In these experiments, the dislocation-originated SFT are observed in nine individual samples, and dislocation interactions alone are observed in two samples with no SFT formation. Therefore, it can be concluded that the dislocation-originated SFT are frequently observed in the deformation of Au nanocrystals and should be considered as an essential deformation mechanism at this length scale.

### Supplementary Note 1: Equation for the dislocation reactions

Following are the equations for the dislocation reactions depicted in Fig. 2f-g in the manuscript.

1. Two Shockley partial dislocations of the  $1/6\langle 112 \rangle$  type react to form a sessile stair-rod dislocation of the  $1/6\langle 110 \rangle$  type (Fig. 2f), as follows:

$$\frac{1}{6}\langle \bar{1}2\bar{1} \rangle + \frac{1}{6}\langle \bar{1}12 \rangle \rightarrow \frac{1}{6}\langle 011 \rangle$$

$$\beta A + \gamma A \rightarrow \beta\gamma$$

$$\delta A + \beta A \rightarrow \delta\beta$$

$$\gamma A + \delta A \rightarrow \gamma\delta$$

2. One of the trailing partials  $\delta B$ , cross-slips into the basal plane BCD (Fig. 2h) producing three partials with equivalent burgers vectors (as they are all in the plane orthogonal to the loading direction and hence have zero Schmid factors)

$$\delta B \xrightarrow{\text{cross-slip into BCD}} B\alpha, C\alpha, D\alpha$$

Each of the three partials in BCD react with the other trailing partials to form the three stair-rod dislocations  $\beta\alpha$ ,  $\delta\alpha$ , and  $\gamma\alpha$ , constituting the base BCD of the SFT:

$$\gamma D + D\alpha \rightarrow \gamma\alpha \quad (\text{along BD})$$

$$\beta C + C\alpha \rightarrow \beta\alpha \quad (\text{along DC})$$

$$\delta B + B\alpha \rightarrow \delta\alpha \quad (\text{along CB})$$

## **Supplementary Note 2: Sample size effects on the SFT formation**

To study the sample size effect, we conducted MD simulations for Au nanowires of various sizes and found that SFT were formed in all of them, following surface dislocation nucleation and interaction events. Supplementary Fig. S7-8 show some SFT observed in Au nanocrystals with different sizes in experiments and Supplementary Fig. S9 shows an example of SFT formation in a larger nanowire in MD simulation. In Supplementary Fig. S9, three SFT can be seen formed in (a), as well as in (b) where atoms are reduced so as to make the view comparable to the TEM image. The atomic structure viewed from a different direction in (c-d) demonstrates that those SFT are fully developed but not inter-connected. The SFT in this larger nanowire (Supplementary Fig. S9) consists of 7 atomic layers, and is slightly larger than those (5 atomic layers) in smaller nanowires presented in Fig. 2 of the main text. Also, multiple SFT can be generated in the samples with larger size (Supplementary Fig. S9). This result proves that the mechanism of SFT formation proposed in our work is not limited to the specific set of dimensions of the nanowire and the size of SFT depends on the sample size. Thus it can be safely concluded that sufficient dislocation activity in FCC metallic nanocrystals can lead to the formation of dislocation-originated SFT through the mechanism we have discovered in our work.